Mie Scattering With and Without Diffraction

Christian Mätzler

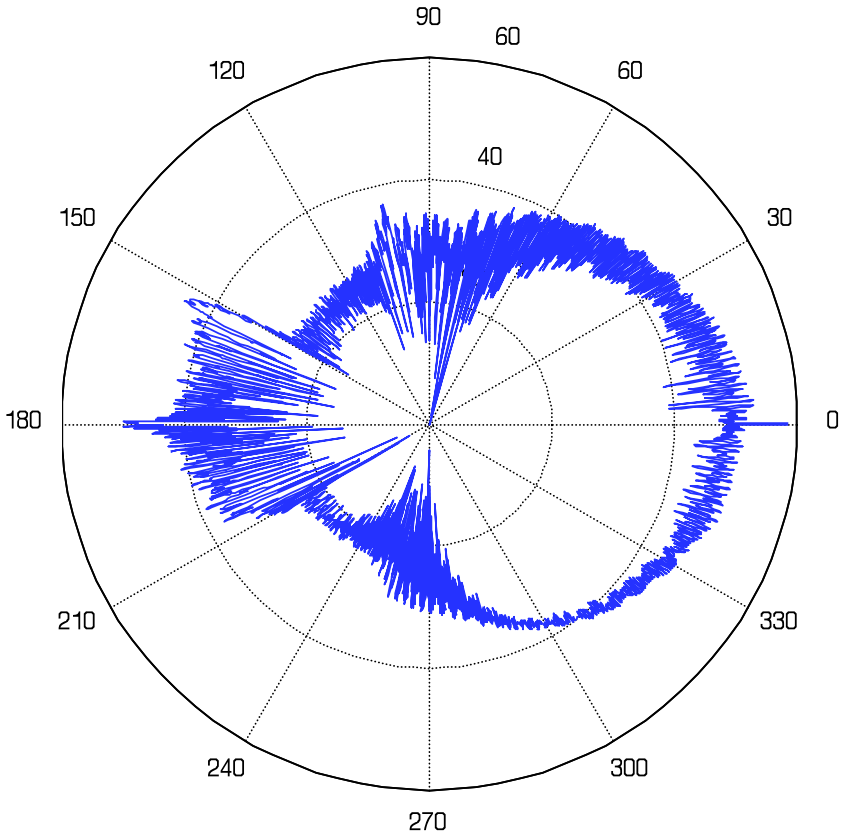

Research Report No. 2004-02
June 2004

Institute of Applied Physics
University of Bern

Microwave Group

Sidlerstrasse 5
3012 Bern
Schweiz

Tel. : +41 31 631 89 11
Fax. : +41 31 631 37 65
E-mail : matzler@iap.unibe.ch

Mie Scattering With and Without Diffraction

Fun with MATLAB Functions

Christian Mätzler, June 2004

Abstract

MATLAB Functions for studying and handling the angular distribution of Lorenz-Mie scattering are introduced and illustrated by situations of low-loss dielectric spheres with size parameters ranging from the Rayleigh to the geometrical-optics regime. Special attention has been paid to the forward peak of the phase function arising from diffraction for large size parameters. This peak causes problems in applications with limited angular resolution. Here the standard computations have been complemented by those without the diffracted signal component. In this way the peak can be avoided without affecting the scattering in other directions. Additional parameters introduced are the beam efficiency, the diffraction efficiency, and the decomposition of the phase functions into Legendre Polynomials. The new option is of benefit in radiative transfer to better take into account effects of scattering at limited angular resolution. The method can be generalised to other types of particles.

Contents

1. Introduction

A MATLAB software for computations of scattering and absorption of radiation interacting with dielectric and magnetic, homogeneous and coated spheres was developed by Mätzler (2002a,b), based on the excellent textbook on this subject by Bohren and Huffman (1983). Here we present and discuss additional functions (s. Appendix) for quantifying and visualising the angular behaviour of Lorenz-Mie scattering (or simply Mie scattering) on dielectric spheres. The new functions can be adapted to magnetic and to coated spheres. Input parameters are the complex refractive index $m=m'+im''$ and the size parameter $x=2\pi a/\lambda$, where λ is the vacuum wavelength and a the sphere radius.

In the first part, results obtained with the function *mie_tetascanall* to plot the angular behaviour of scattered intensity and polarisation will be discussed for $m=1.44+10^{-5}$i. The occurrence of scattering phenomena such as rainbows, and their polarisation features will be shown.

In the second part, attention is paid to the forward peak of the scattering function for large x. For this purpose the concept of beam efficiency is introduced. The forward peak is the result of diffraction at the circular disk representing the projection of the sphere. Indeed, the occurrence of diffraction in addition to scattering is an expression of the well-known extinction paradox. This paradox appears when one realises that the extinction is twice the radiation falling on a particle (van de Hulst, 1957, p. 107). By subtracting the diffraction signal from the scattering amplitudes, a scattering function without forward peak is obtained which coincides with the Mie scattering function in directions outside the peak. The omission of the peak is needed in radiative transfer models (Meador and Weaver, 1980) which consider scattering functions not too different from isotropic ones. Furthermore the omission is needed in the interpretation of scattering and extinction measurements with limited angular resolution, such as sun photometry.

In the third part, phase functions are given for Mie scattering with inclusion and with omission of the forward peak, and with their decomposition into Legendre Polynomials. For $x >>1$ the phase functions with diffraction require decomposition into very high-order polynomials with a large number of coefficients (on the order of $2x$). For the phase function without the diffraction peak, the number of significant terms is much less, on the order of 4. This is a great simplification for radiative transfer computations. The method can be applied to other particles with given scattering and diffraction functions.

2. Angular scattering

The scattered far field in spherical coordinates ($E_{s\theta}$, $E_{s\phi}$) for a unit-amplitude incident field (where the time variation $\exp(-i\omega t)$ has been omitted) at a scattering angle θ is given by

$$E_{s\phi} = \frac{e^{ikr}}{ikr}\sin\phi \cdot S_1(\cos\theta);\ E_{s\theta} = \frac{e^{ikr}}{-ikr}\cos\phi \cdot S_2(\cos\theta) \qquad (1)$$

with the scattering amplitudes S_1 and S_2 being functions of the scattering angle (Bohren and Huffman, 1983). $E_{s\theta}$ is the scattered far-field component in the scattering plane, defined by the incident and scattered directions, and $E_{s\phi}$ is the orthogonal component where ϕ is the angle between the incident electric field and the scattering plane. The scattered power is characterised by components S_R and S_L with polarisation perpendicula$R$ and paralle$L$ to the scattering plane.

$$S_R = \frac{|S_1|^2}{\pi x^2} \quad \text{and} \quad S_L = \frac{|S_2|^2}{\pi x^2} \qquad (2)$$

With this normalisation, the integration of the sum $S=S_L+S_R$ over all scattering directions gives the scattering efficiency Q_{sca}.

If the sphere is illuminated by unpolarised light, such as the sun, the scattered light becomes polarised with a degree of linear polarisation ρ:

$$\rho = \frac{S_R - S_L}{S_R + S_L} \qquad (3)$$

As a first task the function *mie_tetascanall* computes the Mie-Scattering Amplitudes and plots their intensities in various ways. Here, the situation for a low-loss medium $m=1.44+10^{-5}$i will be presented

and discussed. The size parameter x is varied from 0.4 to 4000. This means that for a wavelength of 500 nm the sphere radius increases from 32 nm to 0.32 mm. The range covers the transition from Rayleigh scattering to the range where geometrical optics becomes applicable. Standard Mie Efficiencies (computed with `mie(m,x)`, Mätzler, 2002b), the Diffraction Efficiency according to Equation (13), and the anisotropy parameter g of the phase-function are given in Table 1 for $x \geq 1$.

Table 1: Mie Efficiencies Q_j for extinction (j=*ext*), scattering (j=*sca*), absorption (j=*abs*), backscattering (j=*b*) and diffraction (j=*d*), and asymmetry parameter g for m=1.44+10^{-5}i, x=1 to 10^4.

x	Q_{ext}	Q_{sca}	Q_{abs}	Q_b	Q_d	g
1	0.16711	0.16708	0.00003	0.14714	-	0.19335
2	1.36720	1.36711	0.00009	0.17569	-	0.64778
4	3.85533	3.85515	0.00019	0.42531	-	0.78837
10	2.25693	2.25635	0.00059	2.96921	0.52239	0.61738
20	2.62136	2.62050	0.00086	1.79805	1.13990	0.80666
40	2.32944	2.32771	0.00173	6.62629	1.05018	0.80999
100	2.10636	2.10239	0.00397	2.00493	1.01875	0.82599
200	2.00908	2.00193	0.00714	0.12152	0.98010	0.84008
400	2.03543	2.02080	0.01463	9.30592	1.00068	0.84094
1000	2.02624	1.99101	0.03523	21.9324	1.00279	0.84929
2000	2.00434	1.93629	0.06805	13.2710	0.99472	0.85376
4000	2.01376	1.88251	0.13124	5.05702	1.00470	0.86224
10000	2.00597	1.71366	0.29129	8.97102	1.00081	0.87975

Case x=0.4

As shown in Figure 1, the first example with x = 0.4 represents Rayleigh Scattering at its upper limit, i.e. scattering is nearly symmetrical with respect to forward (θ = 0) and backward (θ = 180°) directions, S_R is nearly independent of θ, and S_L shows the cos^2(θ) dependence. The degree of linear polarisation is positive and has a maximum of 1 at θ = 90°.

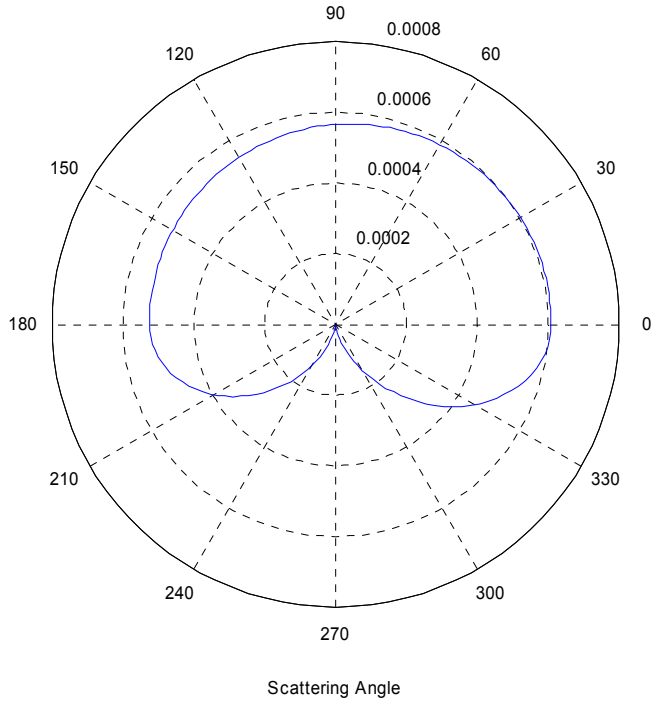

Figure 1: Polar diagram of the Mie scattering functions S_R (upper) and S_L (lower semicircle) in linear scale for size parameter x=0.4, refractive index m=1.44+10^{-5}i.

Case x=4

In contrast to the previous case, the following example with x=4 (Figures 2 and 3) shows scattering minima mainly for S_L, and therefore, the degree of linear polarisation is often negative with an oscillatory behaviour. The number of minima or maxima is closely related to x. Forward scattering is already dominant (asymmetry factor = 0.788).

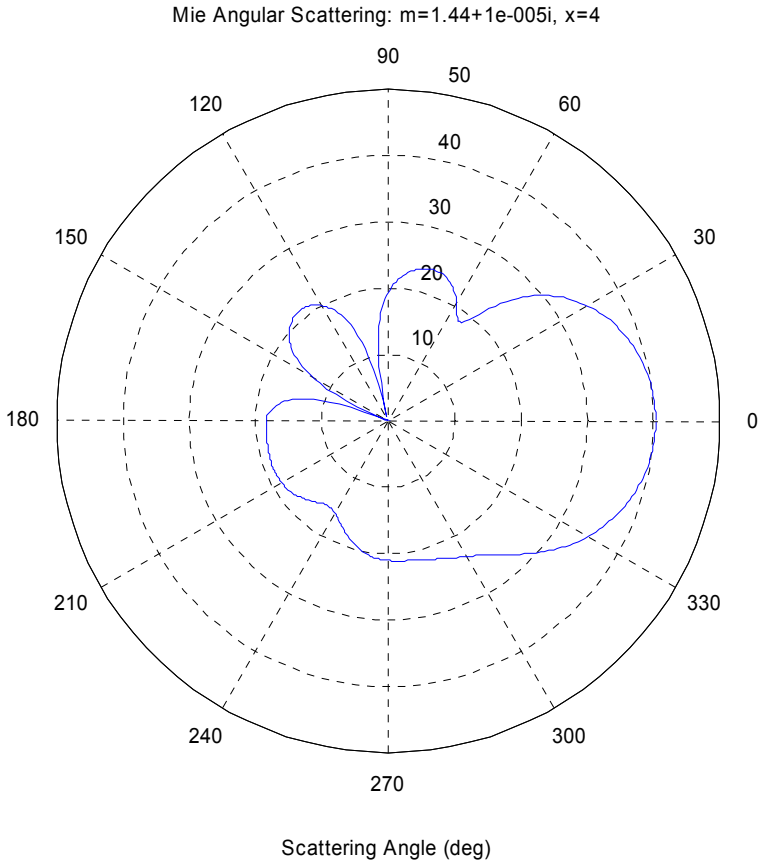

Figure 2:
Polar diagram of the Mie scattering functions S_R (upper) and S_L (lower semicircle) in dB scale and normalised to the minimum value, for size parameter x=4, refractive index m=1.44+10^{-5}i.

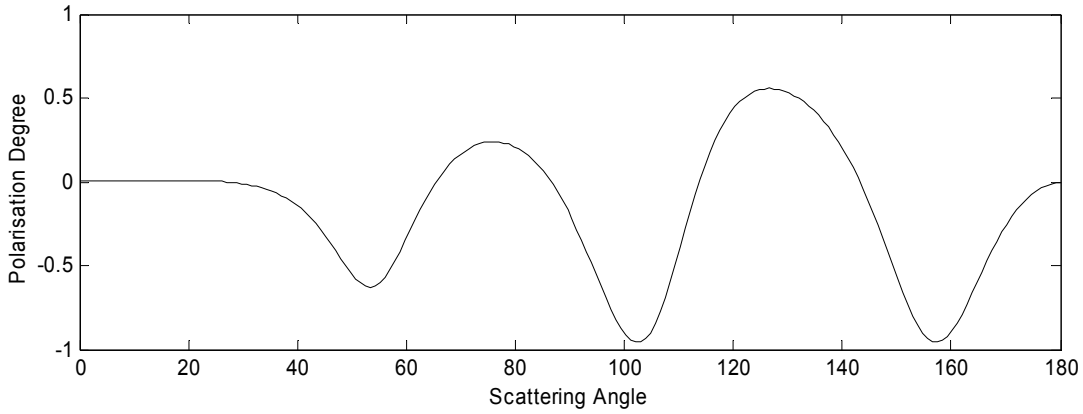

Figure 3: Degree of linear polarisation versus scattering angle, for x=4, m=1.44+10^{-5}i.

Cases *x*=40 to 4000

For x=40 (Figures 4 to 5) the oscillatory behaviour is enhanced, the forward-scattering peak starts to stand out clearly, and a positively polarised rainbow starts to show up for θ between 150° and 160°.
For x=400 (Figures 7 to 8) and even more for x=4000 (Figures 9 to 10), the scattering behaviour more and more approaches the laws of geometrical optics with a superimposed diffraction pattern. This is most apparent in the uppermost graph of Figure 10. In order to reduce the fluctuations due to interference effects the data of S, S_0 and ρ were slightly smoothed with a running average over *nsmooth* values given in the respective figure captions. No smoothing was applied to data shown in polar plots. The diffraction-free scattering function S_0 will be described in Section *Forward Peak*.

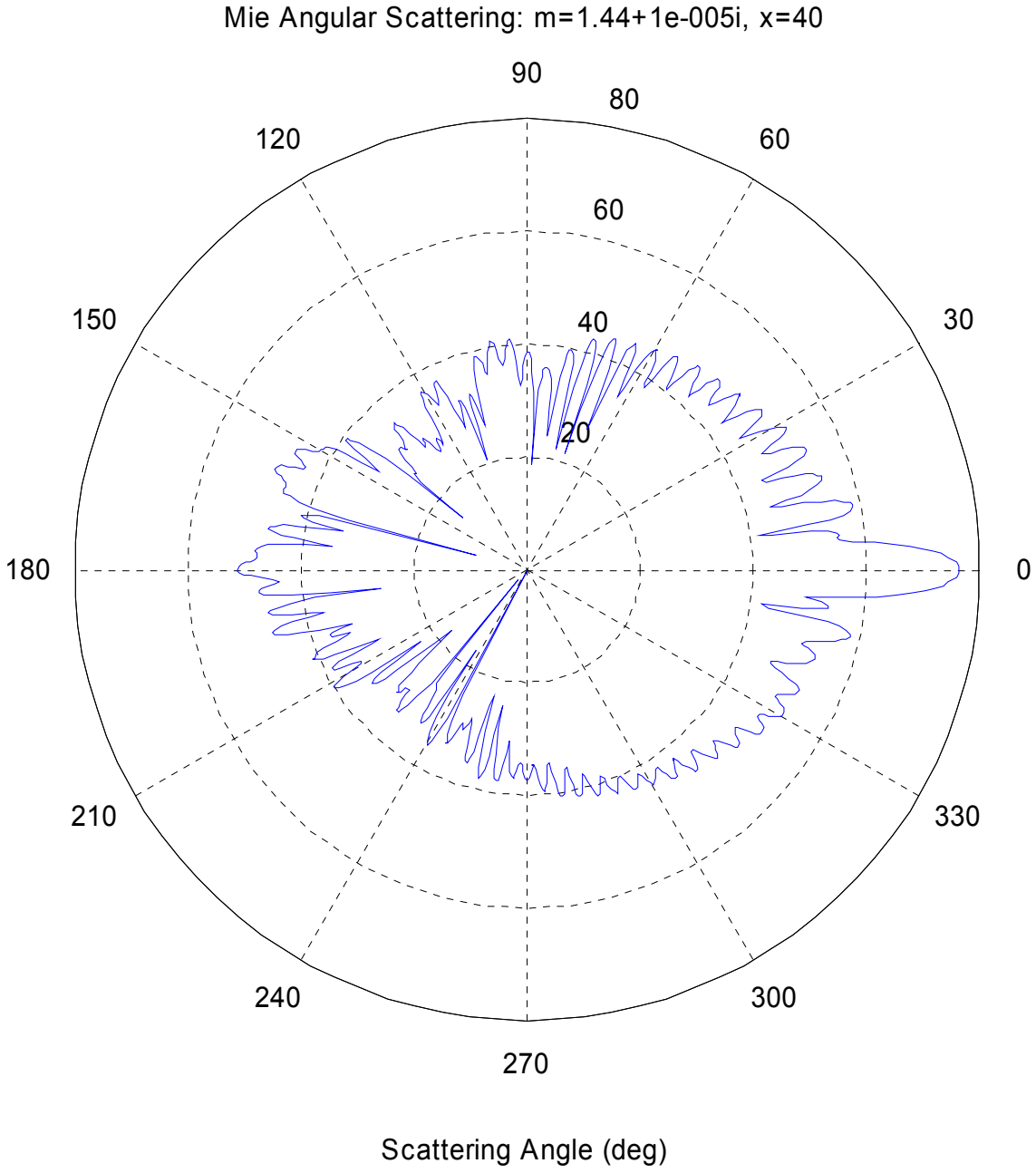

Figure 4: Polar diagram of the scattering functions S_R (upper semicircle) and S_L (lower semicircle) in dB scale and normalised to the minimum value for size parameter x=40, refractive index m=1.44+10^{-5}i.

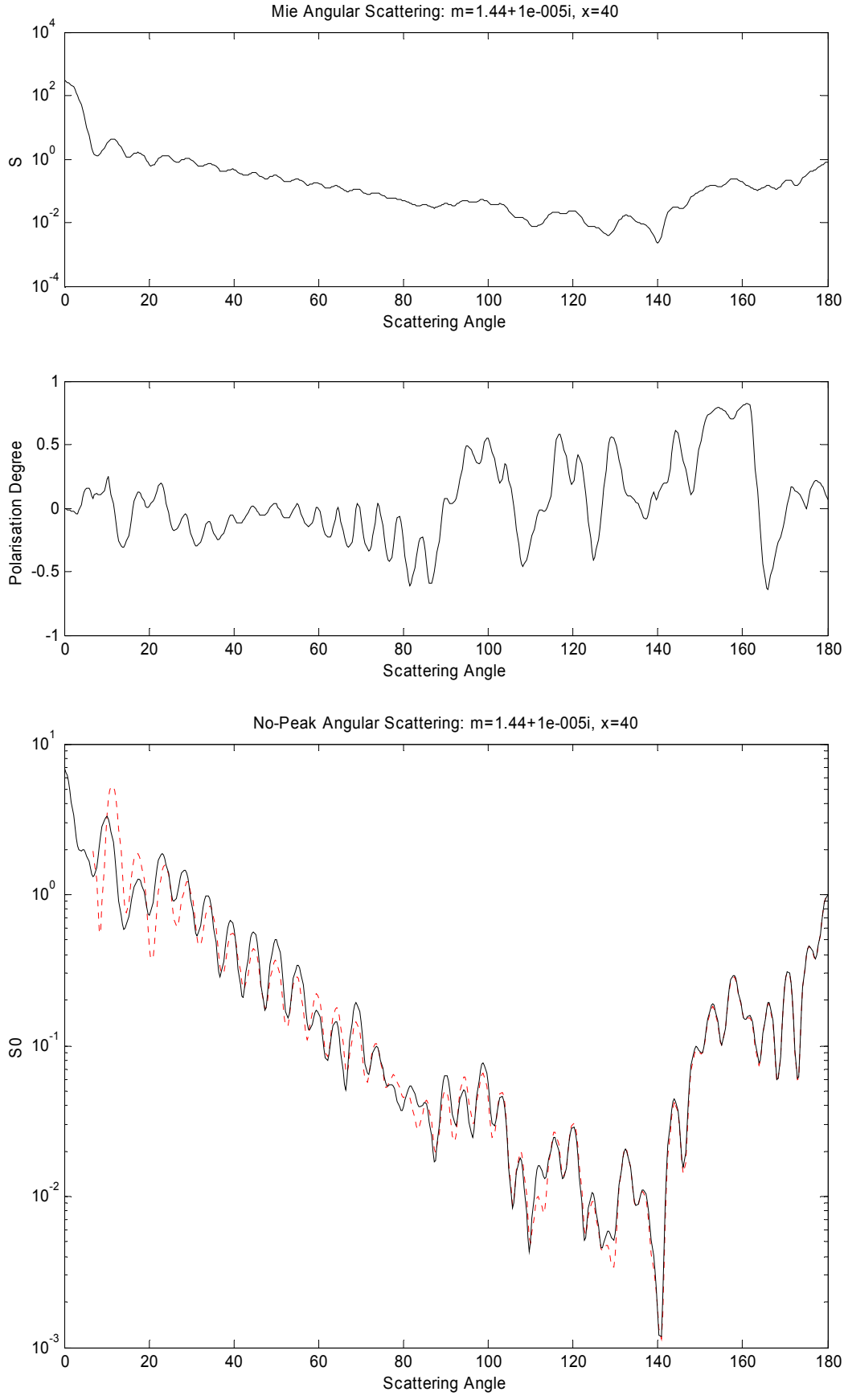

Figure 5: Scattering functions S (top), degree of polarisation (middle graph) and S_0 at bottom graph (black solid line) together with truncated S (red dotted), all versus scattering angle for size parameter x=40. Number of angles: nsteps=500. Smoothing: nsmooth=10, except bottom graph =5.

Rainbows

The first and main rainbow at $\theta = \theta_1 = 151°$ (one internal reflection) and the second rainbow at $\theta = \theta_2 = 105°$ (two internal reflections) are clearly visible as peaks in Figures 8 to 10. Between the two rainbows the scattered intensity is much reduced, whereas outside it is continued by an interference pattern.

The rainbow angles θ_1, θ_2 can be computed in the geometrical optics approximation from the extremes of directions after refractions and internal reflections. The angle θ of rays with j internal reflections is given by (van de Hulst, 1957; Bohren and Huffman, 1983)

$$\theta = \pi + 2[\alpha - (j+1)\beta]; j \text{ odd, else: } \theta = 2[(j+1)\beta - \alpha] \tag{4}$$

where α is the angle of incidence on the sphere, and β is the corresponding angle after refraction to be obtained from Snell's law

$$\sin\beta = \frac{\sin\alpha}{m'} \tag{5}$$

and m' is the real part of the refractive index of the sphere. Rainbows are due to the concentration of rays at positions where $\frac{d\theta}{d\alpha} = 0$, i.e. at angles $\theta = \theta_j$ of (4) with α_j and β_j given by

$$\cos\alpha_j = \sqrt{\frac{m'^2 - 1}{(j+1)^2 - 1}}; \quad \sin\beta_j = \frac{1}{m'}\sqrt{\frac{(j+1)^2 - m'^2}{(j+1)^2 - 1}}; \tag{6}$$

Solutions are obtained for both θ_1 and θ_2 if m' is in the interval $1<m'<2$. This means that the rainbow angles are very sensitive to m'. This is shown in Figure 6 below.

Table 2: Geometrical optics values of the first and second rainbow for m'=1.44.

j	α_j	β_j	θ_j
1	53.26°	33.81°	151.26°
2	68.51°	40.25°	104.50°

For the selected value m'=1.44, the results of Equations (4) to (6) are shown in Table 2. The rainbow angles are near 151° and 104°, and these values agree very well with the positions of the peaks in the Mie results of Figures 9 and 10 (also visible in Figures 7 and 8), not only in the scattered intensity, but also as regions of strongly enhanced polarisation. As a comparison for water with a slightly smaller refractive index (m'=1.34), the rainbows are at the angles of 138.9° and 127.3°, respectively.

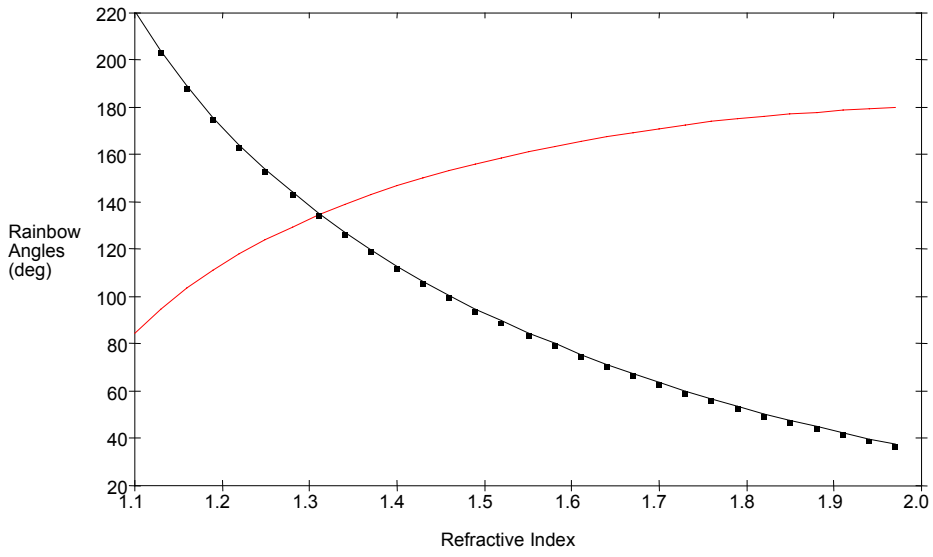

Figure 6: Rainbow angles for first (solid line) and second (pointed) rainbow versus m'.

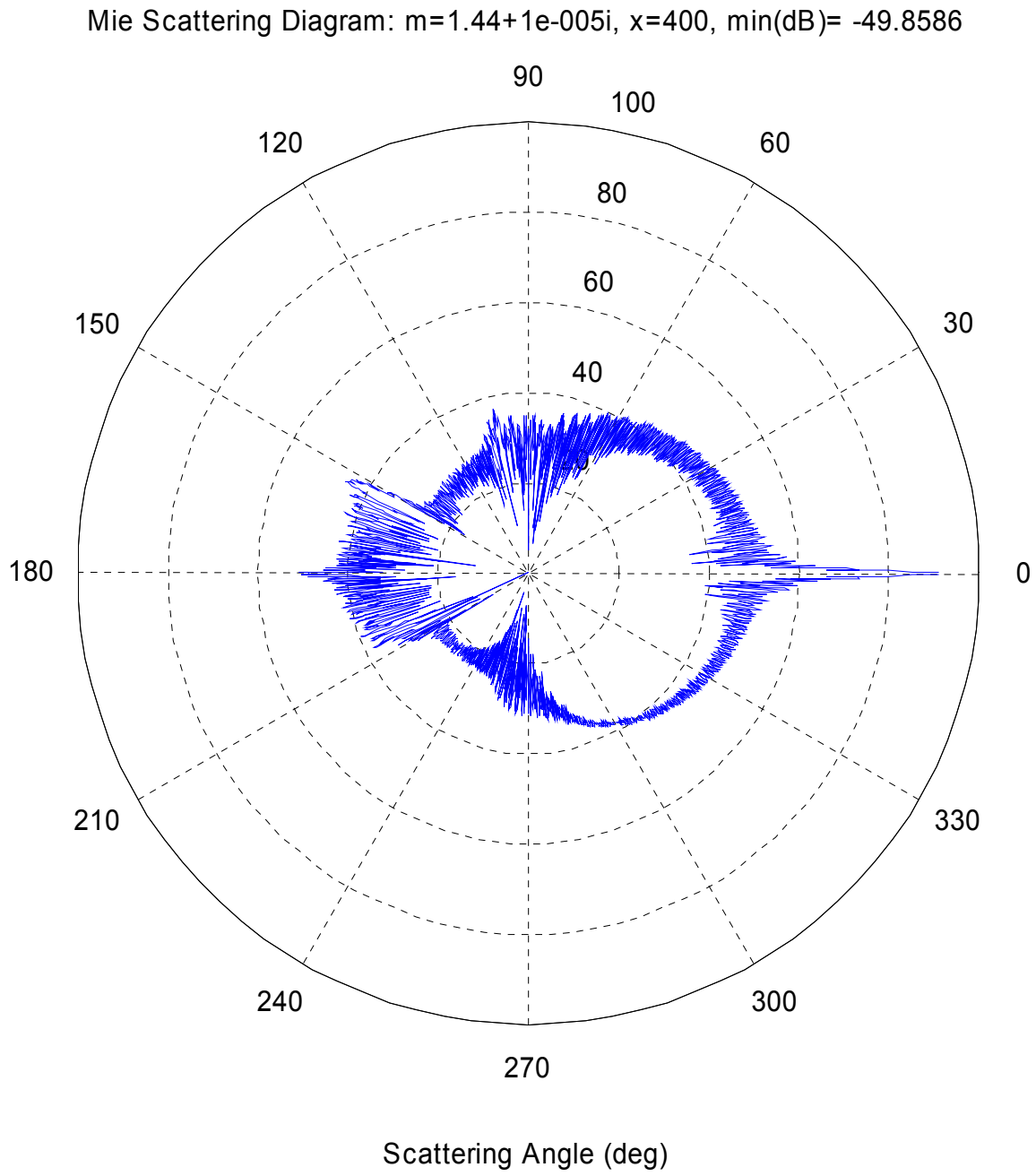

Figure 7a: Polar diagram of the scattering functions S_R (upper semicircle) and S_L (lower semicircle) in dB scale and normalised to the minimum value for size parameter x=400, refractive index m=1.44+10^{-5}i.

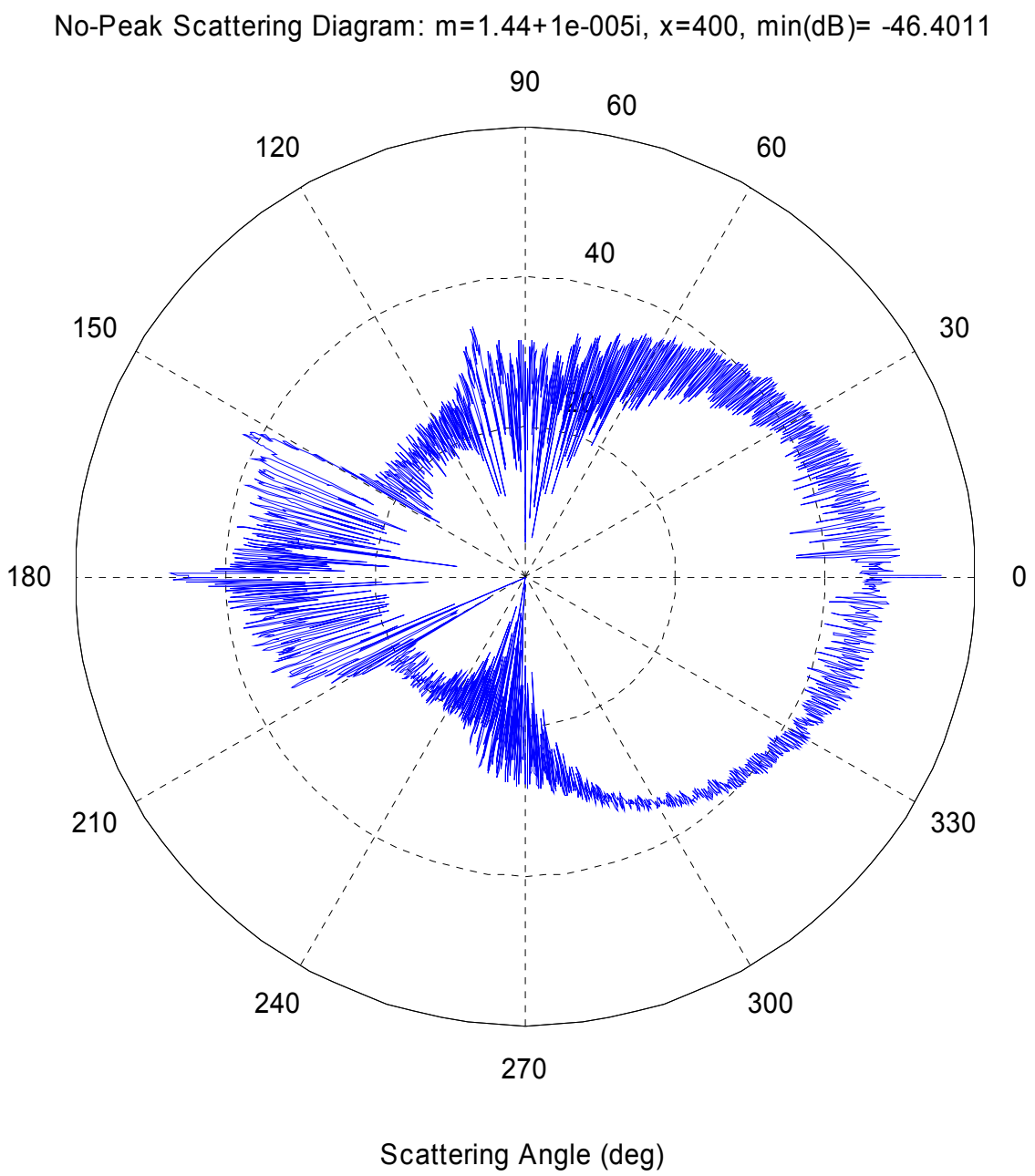

Figure 7b: Polar diagram of the scattering functions without the diffraction signal: S_{R0} (upper semicircle) and S_{L0} (lower semicircle) in dB scale and normalised to the minimum value for size parameter x=400, refractive index m=1.44+10^{-5}i.

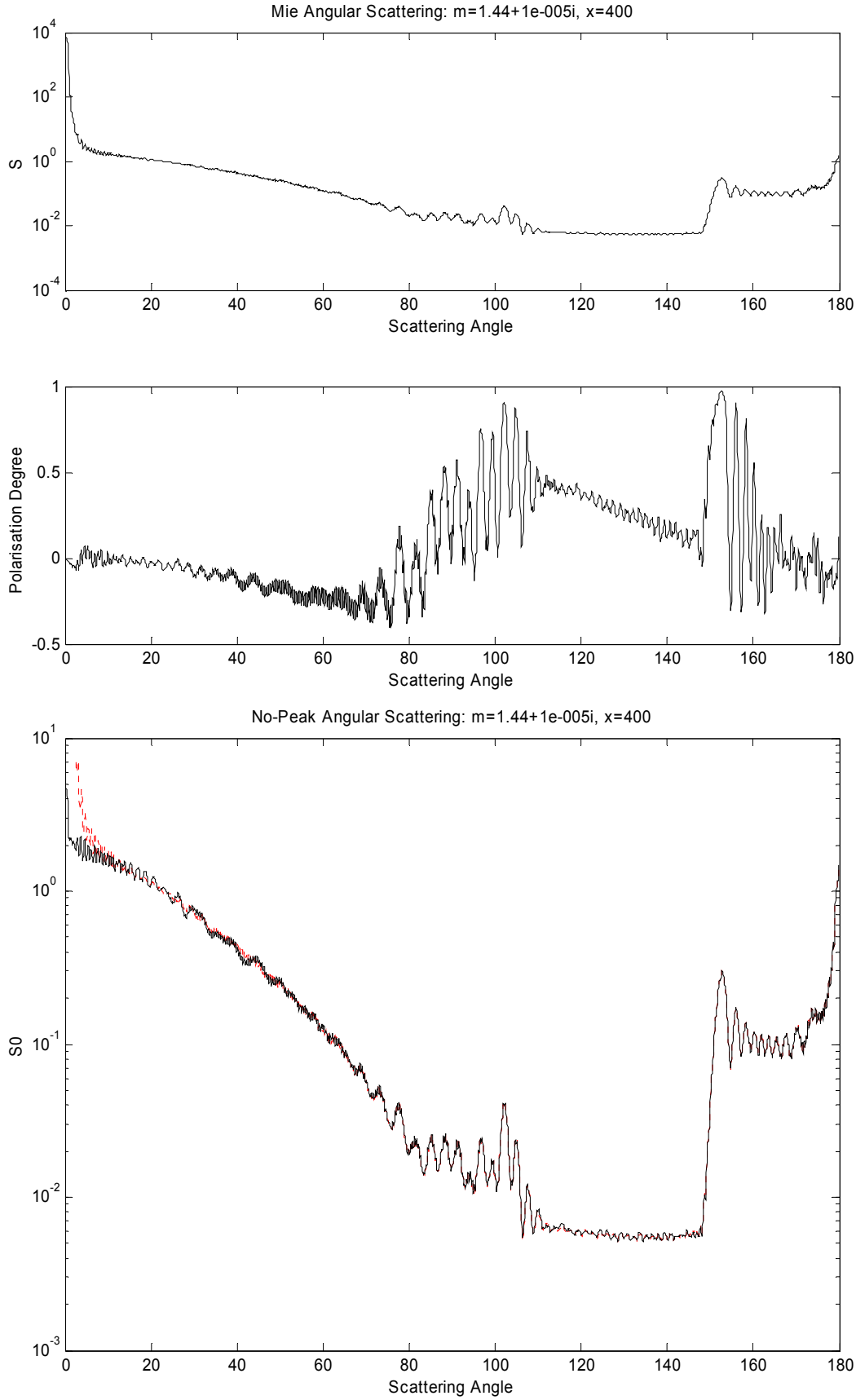

Figure 8: Scattering functions S (top), degree of polarisation (middle graph) and S_0 at bottom graph (black solid line) together with truncated S (red dotted), all versus scattering angle for size parameter x=400. Number of angles: nsteps=3000. Smoothing: nsmooth=20.

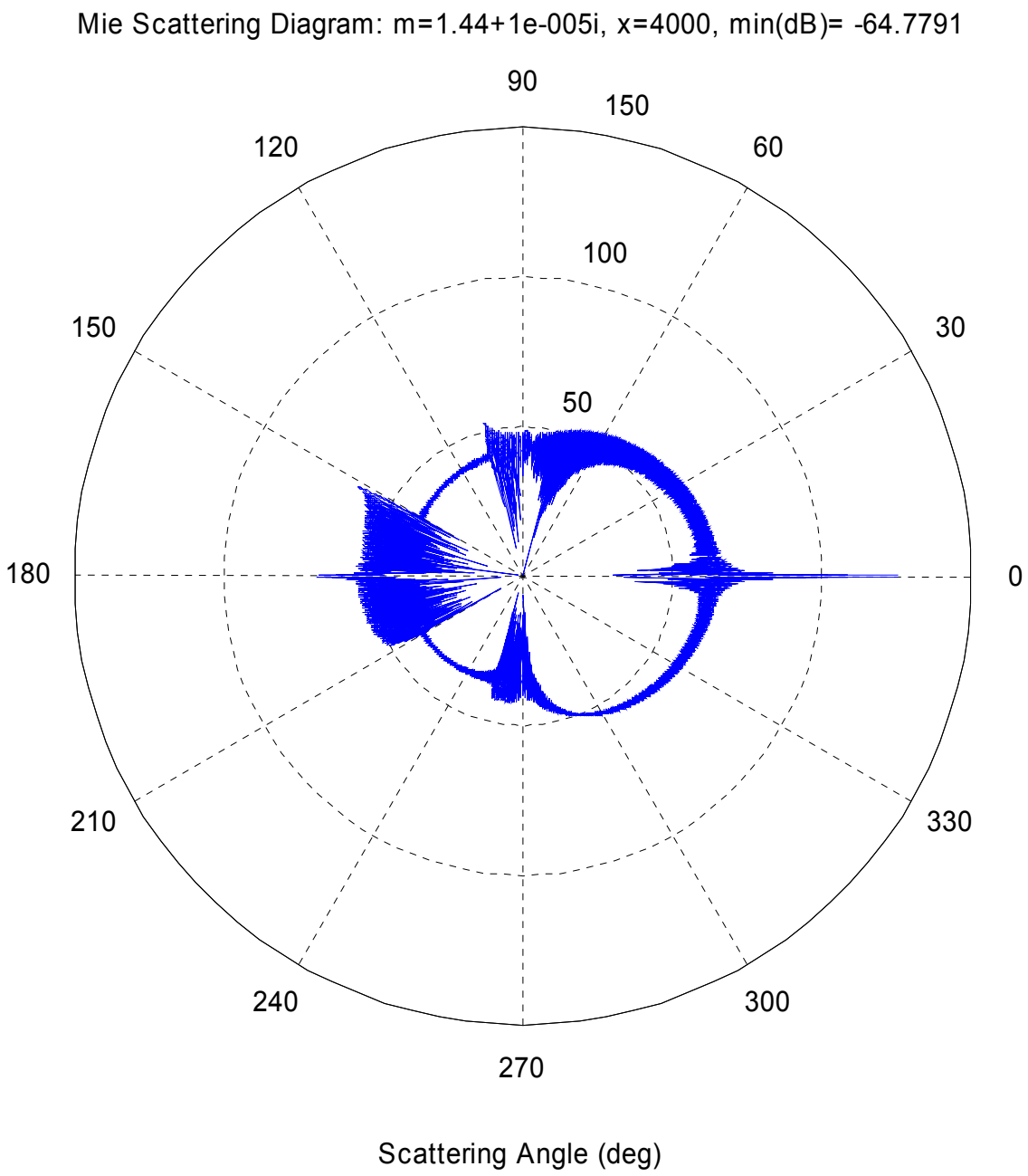

Figure 9a: Polar diagram of S_R (upper semicircle) and S_L (lower semicircle) in dB scale, and normalised to the minimum value for size parameter x=4000, refractive index m=1.44+10^{-5}i.

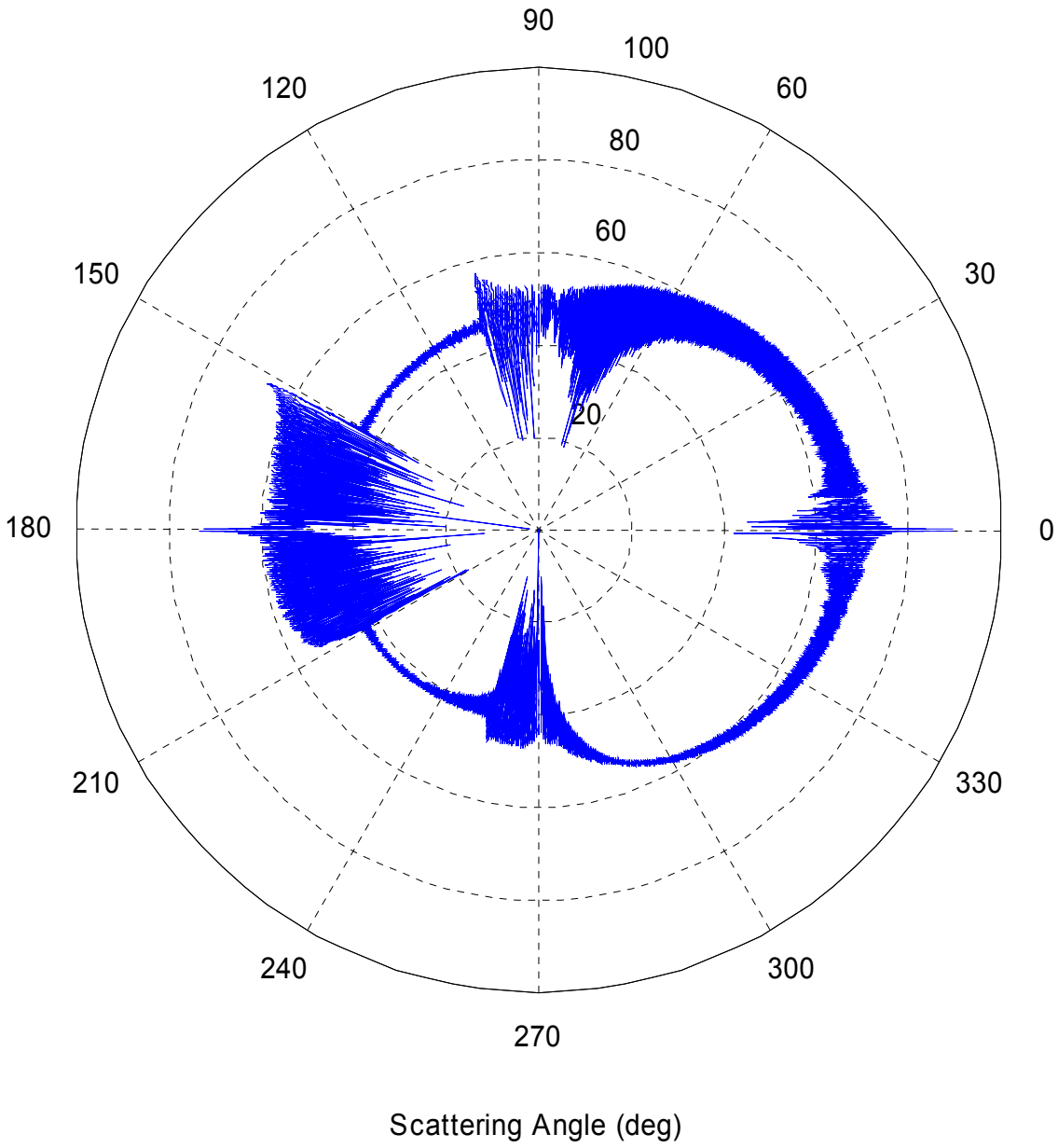

Figure 9b: Polar diagram of the scattering functions without the diffraction signal: S_{R0} (upper semicircle) and S_{L0} (lower semicircle) in dB scale and normalised to the minimum value for size parameter x=4000, refractive index m=1.44+10^{-5}i.

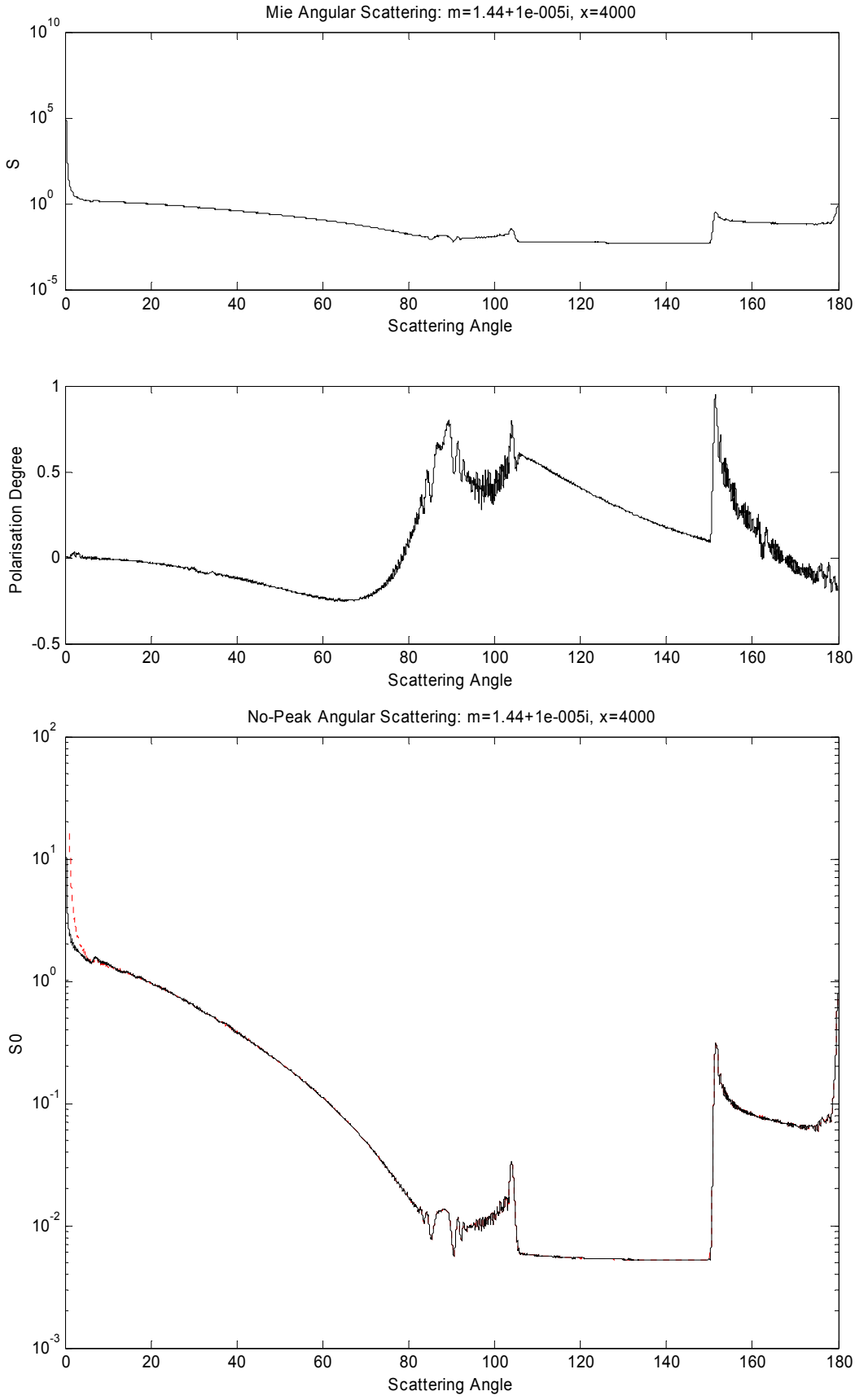

Figure 10: Scattering functions S (top), degree of polarisation (middle graph) and S_0 at bottom graph (black solid line) together with truncated S (red dotted), all versus scattering angle for size parameter x=4000. Number of angles: nsteps=28000. Smoothing: nsmooth=140.

3. Forward peak

Diffraction and its subtraction from the scattering signal

Parts of the scattering functions S_1 and S_2 are due to diffraction of the electromagnetic wave at the projected area of the sphere. This is especially apparent for large x with examples shown in Figures 8 to 10. The diffraction peak is often a disturbing feature when dealing with scattering at a sphere, because scattering in the forward direction does not appear as a scattering loss if the width of the forward peak is narrower than the resolution of the instrument to observe the scattering. Also radiative transfer models computing scattered radiation from slabs of scatterers often are unable to handle strongly peaked scattering functions. Therefore there is a need to separate the diffraction peak from the rest of the scattering function.

The scalar signal representative for a planar, circular diffraction pattern of radius a, size parameter $x=2\pi\, a\,/\lambda$ is given by (Bohren and Huffman, 1983, Section 4.4.3)

$$S_d = x^2 \frac{1+\cos\theta}{2} \cdot \frac{J_1(x\sin\theta)}{x\sin\theta} \tag{7}$$

and the scattering fields without the diffraction pattern - in analogy to Equations (1) - becomes

$$E_{s\phi 0} = \frac{e^{ikr}}{ikr}\sin\phi\cdot(S_1 - S_d);\; E_{s\theta 0} = \frac{e^{ikr}}{-ikr}\cos\phi\cdot(S_2 - S_d) \tag{8}$$

Thus the S_i (i=1,2) in Equations (1) and (2) are to be replaced by the differences $S_{i0} = S_i - S_d$ leading to $S_0 = S_{L0} + S_{R0}$ to get scattering patterns without diffraction. This subtraction is performed at the field level. An alternative would be to subtract the signals at the power level, however, with a poorer quality of the peak removal due to the phase correlation near the forward direction. The MATLAB Function used to compute S_0 is again `mie_tetascanall`, and results are shown in Figures 5, 7 to 10.

Beam Efficiency and Effective Scattering Efficiency

The beam efficiency η_b is a quantity known from antenna theory to describe the fraction of the radiation contained in the main lobe. In analogy, here η_b can be defined as the fraction of radiation scattered in a given angular range, such as the forward peak. This quantity depends on the scattering angle θ_{lim} at the upper limit of integration

$$\eta_b(\theta_{lim}) = \frac{1}{Q_{sca}} \int_0^{\theta_{lim}} S(\theta)\sin\theta\cdot d\theta\,; \quad \eta_{b0}(\theta_{lim}) = \frac{1}{Q_{sca}} \int_0^{\theta_{lim}} S_0(\theta)\sin\theta\cdot d\theta \tag{9}$$

The normalisation of S according to Equation (2) requires η_b =1 for θ_{lim} =π, which was used to test the numerical integration. Two examples with θ_{lim} ranging from very small values to π are shown in Figure 11 for x=400 and 4000. The respective directional integration over S_0 gives η_{b0}; the result is also shown in Figure 11. These values are smaller because the diffraction peak is missing, and $\eta_{b0}(\theta_{lim})$ increases slowly with θ_{lim}, mostly in parallel to η_b beyond the diffraction angles. The difference

$$\eta_{bd} = \eta_b - \eta_{b0} \tag{10}$$

shown as dotted line in the graphs of Figure 11, corresponds to the beam efficiency of the diffraction signal. The dotted curves reach constant values already for small angles, i.e. about 2° for x=400, and 0.2° for x=4000. The width of the diffraction peak is on the order of 180°/x. With increasing x, $\eta_{bd}(\theta_{lim})$ more and more approaches a step function in the semi-logarithmic representation of the graphs in Figure 11, thus indicating a clear distinction between diffraction at small θ_{lim} and more or less diffuse scattering above. A small, but distinct backward peak is also visible for η_b and η_{b0} at the right-hand side of both graphs in Figure 11. This is a manifestation of the glory effect (van de Hulst, 1957).

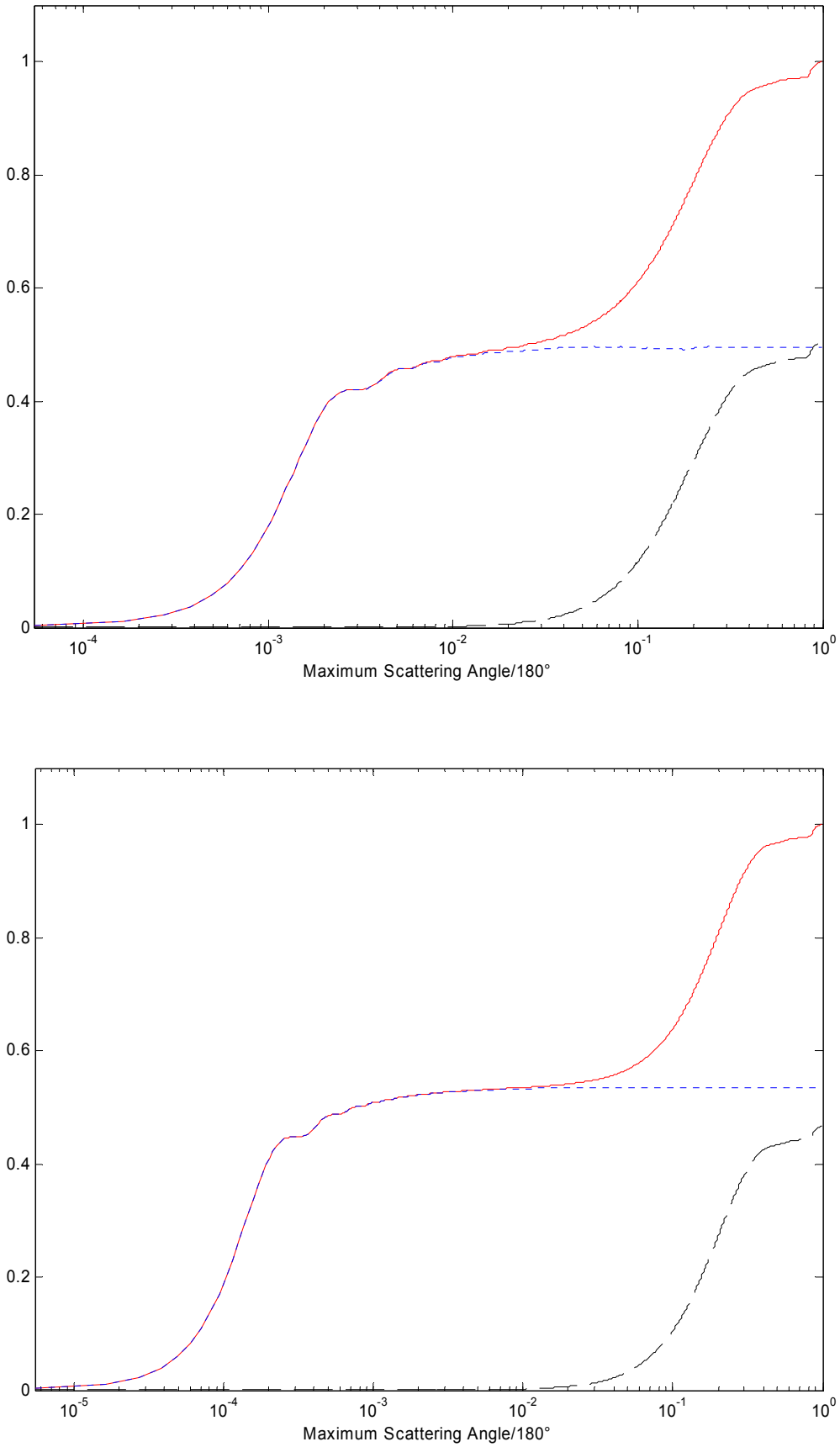

Figure 11: Beam efficiencies η_b (solid line) and η_{b0} (dashed) and their difference (dotted) versus θ_{lim} for size parameter x=400 (upper graph), and for x=4000 (lower graph), refractive index m=1.44+10^{-5}i.

The beam efficiencies can be used to estimate the effective scattering Q_{sca}* and extinction Q_{ext}* efficiencies (the absorption efficiency Q_{abs} being unaffected) from the original values Q_{sca} and $Q_{ext} = Q_{abs} + Q_{sca}$ where only the effect of scattering without diffraction is considered:

$$Q^*_{sca} = Q_{sca} - Q_{sca}\eta_{bd}\,;\;\; Q^*_{ext} = Q_{ext} - Q_{sca}\eta_{bd} \tag{11}$$

Due to the step-like behaviour of η_{bd}, it is possible to avoid its dependence on θ_{lim}, at least for sufficiently large spheres, by choosing the value $\theta_{lim} = \pi$

$$\eta_{bd} = \eta_b(\pi) - \eta_{b0}(\pi) = 1 - \eta_{b0}(\pi) \tag{12}$$

The diffraction efficiency Q_d is related to η_{bd} by

$$Q_d = Q_{sca}\eta_{bd} = Q_{sca} - Q^*_{sca} \quad ; \quad x >> 1 \tag{13}$$

This quantity was computed from (12) by numerical integration according to (9). The results shown in Table 1 indicate that for sufficiently large x, Q_d is very close to 1. This means that $\eta_{bd} \cong 1/Q_{sca}$ and

$$Q^*_{sca} = Q_{sca} - Q_d \cong Q_{sca} - 1\;;\;\; Q^*_{ext} = Q_{ext} - Q_d \cong Q_{ext} - 1 \tag{14}$$

and the effective single-scattering albedo ϖ* becomes

$$\varpi^* = \frac{Q^*_{sca}}{Q^*_{ext}} \cong \frac{Q_{sca} - 1}{Q_{abs} + Q_{sca} - 1} \tag{15}$$

The result is not limited to the special value of m, but is generally valid for sufficiently large x, because the diffraction signal is independent of the physical properties of the sphere. If extinction is understood as the sum of losses by absorption, scattering and diffraction, the well-known extinction paradox (van de Hulst, 1957) is resolved immediately. After subtraction of the diffraction loss, the remaining extinction efficiency approaches $Q^*_{ext} \to Q_{ext} - 1 \to 1$ for $x \to \infty$.

Another example is presented in Table 3 for constant x=200 and variable m', covering the region around $m' = 2$ where the first rainbow merges with the backscatter peak, thus leading to enhanced backscatter; neither g nor Q_d seem to be strongly affected, all situations showing $Q_d \cong 1$.

Table 3: Mie Efficiencies Q_j for extinction (j=*ext*), scattering (j=*sca*), absorption (j=*abs*), backscattering (j=*b*) and diffraction (j=*d*), and asymmetry parameters g for x=200, m=m'+0.001i, where m'=1.2 to 2.5.

m'	Q_{ext}	Q_{sca}	Q_{abs}	Q_b	Q_d	g
1.2	2.099229	1.618585	0.480644	0.56835	1.05774	0.94924
1.3	2.041250	1.551503	0.489747	0.16558	0.97624	0.92507
1.4	2.049675	1.560148	0.489526	0.52057	0.99484	0.90501
1.5	2.075441	1.577244	0.498196	1.11266	1.03103	0.88640
1.6	2.041354	1.544187	0.497167	1.07622	0.97714	0.86441
1.7	2.062153	1.562900	0.499253	15.55968	1.00321	0.85068
1.8	2.067160	1.570164	0.496996	75.28368	1.01404	0.83251
1.9	2.053177	1.544784	0.508393	159.69810	0.99843	0.81382
2.0	2.070283	1.582501	0.487782	41.31594	1.01976	0.80902
2.1	2.062575	1.571687	0.490888	9.49542	1.00679	0.79171
2.2	2.053084	1.565909	0.487174	1.72237	1.00382	0.77902
2.3	2.080204	1.595842	0.484362	0.73189	1.02857	0.77294
2.4	2.032339	1.551666	0.480673	2.54836	0.97723	0.75444
2.5	2.057014	1.579909	0.477104	1.94581	0.99842	0.74733

The MATLAB Function `mie_tetascanall` also computes and plots $\eta_b(\theta_{lim})$ and $\eta_{b0}(\theta_{lim})$.

4. Phase Functions and Related Parameters

Relation between the scattering function *S* and the phase function *p*

The phase function $p(\theta)$ is just another way to express the angular scattering behaviour, and therefore $p(\theta)$ is proportional to $S(\theta)$. Two different normalisations are in use (Chandrasekhar, 1960, p. 6)

$$\frac{1}{2}\int_0^\pi p(\theta)\sin\theta\cdot d\theta = 1 \;\rightarrow\; p(\theta) = \frac{2\pi}{Q_{sca}} S(\theta) \tag{16a}$$

or

$$\frac{1}{2}\int_0^\pi p(\theta)\sin\theta\cdot d\theta = \varpi \;\rightarrow\; p(\theta) = \frac{2\pi}{Q_{ext}} S(\theta) \tag{16b}$$

The factor 2π results from the trivial integration over azimuth. In analogy to (16a,b) the phase function $p^*(\theta)$ without the diffraction signal can be described as

$$p^*(\theta) = \frac{2\pi}{Q^*_{sca}} S_0(\theta) \tag{17a}$$

or

$$p^*(\theta) = \frac{2\pi}{Q^*_{ext}} S_0(\theta) \tag{17b}$$

Asymmetry parameter, and decomposition of *p* and *p** in Legendre Polynomials

The asymmetry parameters g and g^* are defined by

$$g = \frac{1}{2}\int_0^\pi p(\theta)\cos\theta\cdot\sin\theta\cdot d\theta\,;\;\; g^* = \frac{1}{2}\int_0^\pi p^*(\theta)\cos\theta\cdot\sin\theta\cdot d\theta \tag{18}$$

where versions (16a) and (17a) are used for the phase functions. Whereas the standard g can be obtained from the Mie Coefficients (Bohren and Huffman, 1983) without numerical integration, this is not the case for g^*. However, a look at Table 1 shows that g^* is rather constant for $x > 100$, as can be expected from geometrical optics. This is different for g. Therefore g^* does not have to be recomputed for each particle size. This is an advantage for radiative transfer computations.

The asymmetry parameter is the first-order coefficient $g=g_1$ of the decomposition of the phase function into Legendre Polynomials. The decomposition is needed, e.g. in radiative transfer of plane-parallel media, to represent p in terms of functions separable in cosines μ_1 and μ_2 of the incidence angles before and after scattering. The cosine μ of the scattering angle θ can be expressed as

$$\mu = \mu_1\mu_2 + \sqrt{(1-\mu_1)^2(1-\mu_1)^2}\cos\varphi \tag{18}$$

where φ is the change in azimuth during the scattering process. The azimuth-averaged phase function $p(\mu_1, \mu_2)$ can be expressed as (Meador and Weaver, 1980)

$$p(\mu_1,\mu_2) = \frac{1}{2\pi}\int_0^{2\pi} p(\theta(\mu_1,\mu_2,\varphi)d\varphi = \sum(2i+1)g_i P_i(\mu_1)P_i(\mu_2) \tag{19}$$

where P_i are Legendre Polynomials, and the coefficients g_i are given by

$$g_i = \frac{1}{2}\int_{-1}^{1} P_i(\mu)p(\mu)d\mu\,;\; g_i^* = \frac{1}{2}\int_{-1}^{1} P_i(\mu)p^*(\mu)d\mu \tag{20}$$

where $p(\mu) = p(\cos\theta)$. Corresponding coefficients g_i^* also exist for the phase function p^* without the diffraction signal. In addition the normalisation conditions require $g_0 = 1$, and $g_0^* = 1$, and the anisotropy factors should be given by $g = g_1$ and $g^* = g_1^*$. The first ten g_i and g_i^* are shown in Tables 4 and 5 for the examples discussed here. Mie Scattering has significant g_i values up to $i \cong 2{\cdot}x$. On the other hand, with increasing i, the g_i^* values rapidly converge to 0, and values larger than 0.1 are only found up to $i \cong 4$. This demonstrates the main advantage of using p^*.

Table 4a: Asymmetry parameter g and higher g_i coefficients for $i \leq 10$, $m=1.44+10^{-5}$i, $x=10$ to 10^4.

x	g	g_2	g_3	g_4	g_5	g_6	g_7	g_8	g_9	g_{10}
10	0.61747	0.57602	0.39045	0.38745	0.31076	0.31030	0.27748	0.24479	0.22482	0.17664
20	0.80672	0.73158	0.59573	0.55693	0.50515	0.49473	0.48202	0.46684	0.45413	0.43759
40	0.81004	0.73811	0.60121	0.57507	0.51438	0.50291	0.48440	0.46849	0.46192	0.45221
100	0.82603	0.74947	0.60466	0.57118	0.51140	0.50444	0.49075	0.48084	0.47727	0.47078
200	0.84012	0.75929	0.61425	0.57201	0.51758	0.50843	0.49995	0.48831	0.49056	0.48283
400	0.84097	0.76254	0.62142	0.58062	0.52610	0.51771	0.51019	0.49938	0.50102	0.49341
1000	0.84932	0.76994	0.63216	0.58795	0.53733	0.52819	0.52308	0.51109	0.51476	0.50674
2000	0.85380	0.77290	0.63778	0.59223	0.54385	0.53440	0.53019	0.51841	0.52249	0.51454
4000	0.86227	0.78155	0.65361	0.60786	0.56339	0.55403	0.55038	0.53910	0.54324	0.53576
10000	0.87977	0.80045	0.68923	0.64485	0.60833	0.59995	0.59664	0.58769	0.59073	0.58513

Table 4b: Same as Table 4a, but for g^* and higher g_i^* coefficients.

x	g^*	g_2^*	g_3^*	g_4^*	g_5^*	g_6^*	g_7^*	g_8^*	g_9^*	g_{10}^*
10	0.4723	0.3581	0.0743	0.0398	-0.0514	-0.0128	-0.0114	-0.0069	0.0113	-0.0138
20	0.6190	0.4452	0.1584	0.0655	-0.0233	-0.0163	0.0019	0.0150	0.0295	0.0357
40	0.6335	0.4837	0.2140	0.1580	0.0472	0.0356	0.0180	0.0050	0.0091	0.0065
100	0.6583	0.5107	0.2296	0.1673	0.0534	0.0430	0.0211	0.0072	0.00765	0.0020
200	0.6871	0.5298	0.2478	0.1669	0.0613	0.0436	0.0268	0.0043	0.0097	-0.0029
400	0.6858	0.5318	0.2544	0.1749	0.0675	0.0500	0.0338	0.0107	0.0130	-0.0019
1000	0.6958	0.5357	0.2577	0.1684	0.0661	0.0473	0.0368	0.0121	0.0195	0.0032
2000	0.6990	0.5321	0.2537	0.1596	0.0598	0.0401	0.0314	0.0072	0.0156	-0.0070
4000	0.7043	0.5308	0.2560	0.1575	0.0620	0.0418	0.0340	0.0098	0.0187	0.0026
10000	0.7109	0.5201	0.2526	0.1457	0.0578	0.0376	0.0297	0.0082	0.0155	0.0020

Table 5a: Asymmetry parameter g and higher g_i coefficients for $i \leq 10$, $x=200$, $m = m' + 0.001i$, for variable m'.

m'	g	g_2	g_3	g_4	g_5	g_6	g_7	g_8	g_9	g_{10}
1.2	0.9493	0.9033	0.8478	0.7925	0.7499	0.7217	0.6954	0.6798	0.6687	0.6584
1.3	0.9251	0.8635	0.7876	0.7291	0.6966	0.6698	0.6577	0.6497	0.6408	0.6382
1.4	0.9050	0.8344	0.7483	0.7042	0.6740	0.6599	0.6545	0.6453	0.6432	0.6386
1.5	0.8864	0.8111	0.7213	0.6940	0.6651	0.6650	0.6545	0.6533	0.6489	0.6462
1.6	0.8644	0.7823	0.6924	0.6782	0.6512	0.6586	0.6410	0.6474	0.6371	0.6415
1.7	0.8507	0.7703	0.6848	0.6788	0.6526	0.6649	0.6453	0.6570	0.6406	0.6498
1.8	0.8325	0.7499	0.6705	0.6707	0.6478	0.6619	0.6449	0.6580	0.6393	0.6492
1.9	0.8139	0.7335	0.6640	0.6716	0.6508	0.6623	0.6442	0.6557	0.6384	0.6486
2.0	0.8091	0.7298	0.6651	0.6720	0.6519	0.6602	0.6433	0.6524	0.6379	0.6459
2.1	0.7918	0.7156	0.6571	0.6661	0.6467	0.6550	0.6394	0.6472	0.6345	0.6406
2.2	0.7791	0.7055	0.6531	0.6635	0.6456	0.6525	0.6393	0.6448	0.6345	0.6380
2.3	0.7730	0.7027	0.6583	0.6677	0.6525	0.6567	0.64734	0.6495	0.6428	0.6432
2.4	0.7545	0.6858	0.6456	0.6556	0.6409	0.6439	0.6361	0.6372	0.6316	0.6312
2.5	0.7474	0.6846	0.6487	0.6592	0.6447	0.6480	0.6405	0.6414	0.6357	0.6357

Table 5b: Same as Table 5a, but for g^* and higher g_i^* coefficients.

m'	g^*	g_2^*	g_3^*	g_4^*	g_5^*	g_6^*	g_7^*	g_8^*	g_9^*	g_{10}^*
1.2	0.8544	0.7255	0.5721	0.4209	0.3059	0.2307	0.1591	0.1159	0.0842	0.0538
1.3	0.7928	0.6192	0.4073	0.2439	0.1528	0.0800	0.0505	0.0348	0.0187	0.0201
1.4	0.7338	0.5345	0.2930	0.1692	0.0848	0.0472	0.0355	0.0152	0.0156	0.0094
1.5	0.6733	0.4587	0.2044	0.1297	0.0482	0.0470	0.0153	0.0110	0.0002	-0.0017
1.6	0.6240	0.3911	0.1375	0.0932	0.0181	0.0407	-0.0012	0.0229	0.0014	0.0183
1.7	0.5775	0.3468	0.1021	0.0825	0.0081	0.0442	-0.0073	0.0300	-0.0110	0.0208
1.8	0.5275	0.2954	0.0735	0.0751	0.0096	0.0469	-0.0026	0.0349	-0.0136	0.0226
1.9	0.4753	0.2511	0.0586	0.0813	0.0211	0.0498	-0.0039	0.0291	-0.0150	0.0224
2.0	0.4630	0.2416	0.0612	0.0809	0.0223	0.0428	-0.0057	0.0221	-0.0125	0.0190
2.1	0.4209	0.2108	0.0500	0.0754	0.0191	0.0387	-0.0060	0.0171	-0.0127	0.0124
2.2	0.3851	0.1828	0.0393	0.0689	0.0169	0.0336	-0.0037	0.0142	-0.0077	0.0112
2.3	0.3619	0.1654	0.0423	0.0686	0.0237	0.0329	0.0061	0.0154	0.0032	0.0135
2.4	0.3352	0.1474	0.0378	0.0635	0.0216	0.0286	0.0077	0.0135	0.0034	0.0089
2.5	0.3087	0.1318	0.0296	0.0561	0.0170	0.0283	0.0114	0.0176	0.0063	0.0116

Phase functions and their g_i and g_i^* values are computed from S and S_0 using (16) and (17) and the MATLAB Function `mie_tetascanall`. The g_i and g_i^* values alone are computed by `mie_teta` . The Function `mie_phasefunction` can be used to compute the phase function alone.

5. Discussion

The problem of the forward peak was noted already many years ago. A well-known method to treat the problem in simplified radiative transfer of multiply scattering media has been the Delta-Eddington Approximation of Joseph et al. (1976) who represented the forward peak by a weighted delta function, and the remaining scattering function was assumed to be given by a constant term plus a term linear in cosθ. This allows to use the normal Eddington Approximation for the scattering without the delta function but with modified parameters g_{DE}* correspondingly as g* of the previous section, and similarly for the other parameters; the following relationships were proposed by Joseph et al. (1976)

$$g_{DE}^{*} = \frac{g}{g+1} \quad ; \; Q_{ext,DE}^{*} = Q_{ext}(1-\varpi g^2) \; ; \; Q_{sca,DE}^{*} = Q_{sca}(1-g^2) \qquad (21)$$

where $\varpi = Q_{sca}/Q_{ext}$ is the single scattering albedo of the original parameters. This transformation can be checked by comparing g_{DE}* data with those of g* for given g. The case with m =1.44+0.00001i is shown in Figure 12. The Delta-Eddington values are significantly lower than the numerically computed g* and Q_{sca}*. This discrepancy is an expression of the rather poor representation of the phase function by the Delta Eddington Approximation.

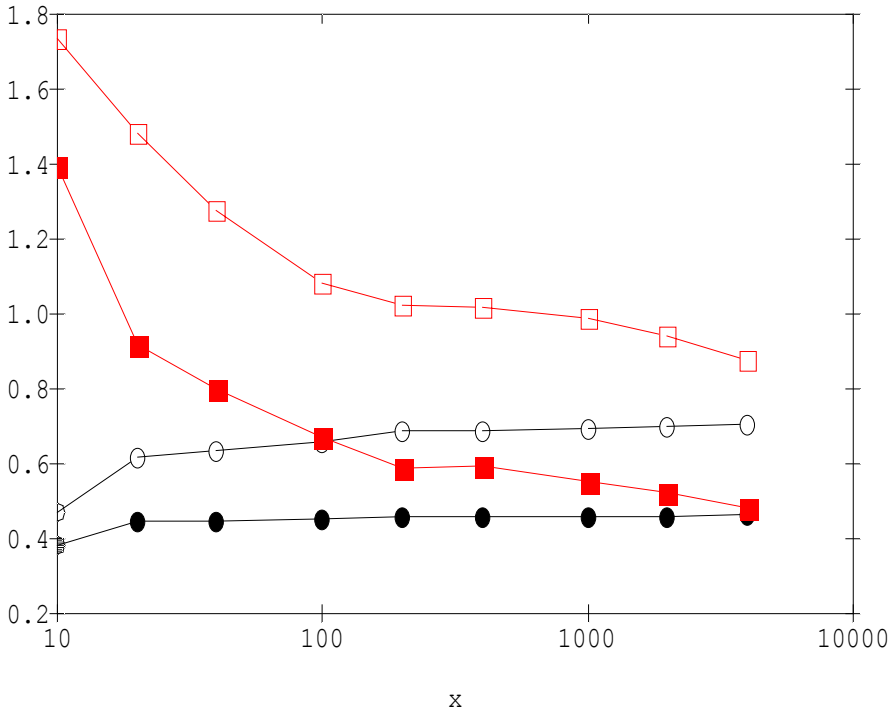

Figure 12:
Comparison of g* (open circles) and Q_{sca}* (open squares) with g_{DE}* (full circles) and $Q_{sca,DE}$* (full squares) versus x for m=1.44+0.00001i.

A different approximation was proposed by Meador and Weaver (1980) by their Modified-Eddington-Delta-Function Hybrid Method. It was estimated to be superior to the Delta-Eddington Approximation, but a direct comparison as in Figure 12 has not been given. For further delta methods, see Thomas and Stamnes (1999).

6. Conclusions

New MATLAB Functions have been presented to visualise and to study the angular behaviour of Lorenz-Mie Scattering of dielectric spheres with emphasis on large size parameters with concentration on low loss dielectric media with refractive index mostly below 2. Special effects, such as rainbows, can be described in detail, including the behaviour of polarisation. Attention has been paid to the forward peak of the phase function arising from diffraction. This peak is a handicap in applications and in measurements with limited angular resolution, and it is the reason for the well-known extinction paradox. If the scattering angle is smaller than the angular resolution, the scattered radiation appears as if it had not been scattered. Only after a large number of forward-scattering events will the photons travel in an appreciably different direction. In order to take this limitation into account, the Mie scattering amplitudes have been presented with and without the diffraction peak. Beam efficiencies were introduced to find the critical transition angle between the peak and the effective scattering regime. Significant differences were found for large size parameters between the phase functions with and without the diffraction signal. In the former case the peak is responsible for a large number of significant coefficients g_i when decomposed into Legendre Polynomials, whereas in the latter case, only a few significant g_i* terms occur. Furthermore the dependence on size parameter was found to be weak. Apart from certain details, the main conclusions also apply to other values of the refractive index. Especially for absorbing spheres, the situation is even simpler due to smoother phase functions.

A further improvement can be introduced by a user-selected value of the limiting scattering angle θ_{lim} in Equations (9) to (13). This option – already realised in `mie_teta` (s. Appendix) – is useful if the limiting angle is specified by the experimental or computational setup. The modification gives adapted values of η_{bd} and Q_d (`etabdlim`, `Qdlim`).

References

Bohren C.F. and D.R. Huffman, “Absorption and scattering of light by small particles”, John Wiley, New York, NY (1983).

Chandrasekhar S., "Radiative Transfer", Dover Publication (1960).

van de Hulst H.C. “Light scattering by small particles”, Dover Publications, New York, NY (1957).

Joseph, J.H, W.J. Wiscombe and J.G. Weinman, “The Delta-Eddington Approximation for radiative flux transfer”, J. Atmosph. Sci. 33, 2452-2459 (1976).

Mätzler C., “MATLAB Functions for Mie Scattering and Absorption”, IAP Res. Rep. No. 02-08, Institute of Applied Physics, University of Bern, June (2002a).

Mätzler C. “MATLAB Functions for Mie Scattering and Absorption, Version 2”, IAP Res. Rep. No. 02-11, Institute of Applied Physics, University of Bern, August (2002b).

Meador W.E. and W.R. Weaver, “Two-stream approximations to radiative transfer in planetary atmospheres: A unified description of existing methods and a new improvement”, J. Atmosph. Sci. Vol. 37, pp. 630-643 (1980).

Appendix: MATLAB Functions

The following new MATLAB functions together with those of Version 2 (Mätzler, 2002b) including minor modifications form the set of MATLAB Lorenz-Mie Functions of Version 3. These functions can be obtained from the author.

The MATLAB Function *mie_tetascanall*

```
function result = mie_tetascanall(m, x, nsteps, nsmooth, type)

% Computation and plot of Mie Power Scattering and diffraction functions
% for complex refractive-index ratio m=m'+im", size parameters x=k0*a,
% according to Bohren and Huffman (1983) BEWI:TDD122
% 1) polar diagram, linear or in dB scale with respect to minimum, with
% SL in upper semicircle, SR in lower semicircle and 3 cartesian diagrams
% 2) same for SL0 and SR0 without diffraction pattern,
% 3) scattered intensity S (lin or log scale), and degree of polarisation
% 4) scattered intensity without diffraction peak S0 (lin or log scale),
% 5) beam efficiencies of S and S0, diffraction efficiency Qd
% 6) gi-factors (coefficients of Legendre Polynomials of Phase Function).
% nsteps: number of scattering angles (for accurate comp. use nsteps=22*x)
% nsmooth: number of values to be averaged in polarisation, S and S0
% (for 'log' type only)
% type:= 'log' or 'lin' for logarithmic or linear plots
% C. Matzler, April 2004.

nstart=round(min(0.5*nsteps,nsteps*pi/x+nsmooth));
m1=real(m); m2=imag(m);
nx=(1:nsteps); dteta=pi/nsteps;
Q=mie(m,x);  Qext=Q(1); Qsca=Q(2); Qabs=Q(3); Qb=Q(4); asy=Q(5);
nmax=round(2+x+4*x^(1/3));
ab=mie_ab(m,x); an=ab(1,:); bn=ab(2,:);
teta=(nx-0.5).*dteta; tetad=teta*180/pi;
u=cos(teta); s=sin(teta);
px=pi*x^2;
st=pi*s*dteta/Qsca;
for j = 1:nsteps,
    pt=mie_pt(u(j),nmax);
    pin =pt(1,:);
    tin =pt(2,:);
    n=(1:nmax);
    n2=(2*n+1)./(n.*(n+1));
    pin=n2.*pin; tin=n2.*tin;
    S1=(an*pin'+bn*tin');
    S2=(an*tin'+bn*pin');
    xs=x.*s(j);
    if abs(xs)<0.00002         % Diffraction pattern according to BH, p.
110
        S3=x.*x*0.25.*(1+u(j));    % avoiding division by zero
    else
        S3=x.*x*0.5.*(1+u(j)).*besselj(1,xs)./xs;
    end;
    S4=S1-S3;
    S5=S2-S3;
    SR(j)= real(S1'*S1)/px;
    SL(j)= real(S2'*S2)/px;
    SD(j)= real(S3'*S3)/px;
    SR0(j)=real(S4'*S4)/px;
    SL0(j)=real(S5'*S5)/px;
end;
z=st.*(SL+SR);
z0=st.*(SL0+SR0);

nj=11;             % Phase fct decomposition in Legendre Polynomials
for jj=1:nj,
    xa=legendre(jj-1,u);
    x0=xa(1,:);
    gi(jj)=x0*z';    % beam efficiency, asymm. factor and higher gi's
    g0i(jj)=x0*z0';  % same as gi's, but diffraction signal removed
```

```
end;
etab=gi(1);     gi=gi/etab;     gi=gi(2:nj);
etab0=g0i(1);   g0i=g0i/etab0;  g0i=g0i(2:nj);
Qd=Qsca*(1-etab0);           % Qd = diffraction efficiency
z=cumsum(z);                 % Beam Efficiency vs. tetalim
z0=cumsum(z0);

S=(SL+SR); S0=(SL0+SR0);     % Intensity
Ss=smooth(S,nsmooth); S0s=smooth(S0,nsmooth);
dS=(SR-SL)./S;          % Degree of polarisation
dSs=smooth(dS,nsmooth);

figure;
if type=='lin'                   % linear plots
    y=[teta teta+pi;SR SL(nsteps:-1:1)]';
    polar(y(:,1),y(:,2)),
    title(sprintf('Mie Scattering Diagram: m=%g+%gi, x=%g',m1,m2,x)),
    xlabel('Scattering Angle'),
figure;
subplot(2,1,1);
    plot(tetad,S,'k-')
    title(sprintf('Mie Angular Scattering: m=%g+%gi, x=%g',m1,m2,x)),
    xlabel('Scattering Angle'),
    ylabel('S');
subplot(2,1,2);
    plot(tetad,dS,'k-')
    xlabel('Scattering Angle'),
    ylabel('Polarisation Degree ');
elseif type=='log',              % logar. plots
    y=[teta teta+pi;10*log10(SR) 10*log10(SL(nsteps:-1:1))]';
    ymin=min(y(:,2));            % Minimum for normalisation of log-polar
plot
    y(:,2)=y(:,2)-ymin;
    polar(y(:,1),y(:,2)),
    title(sprintf('Mie Scattering Diagram: m=%g+%gi, x=%g, min(dB)=
%g',m1,m2,x,ymin)),
    xlabel('Scattering Angle (deg)');
    y=[teta teta+pi;10*log10(SR0) 10*log10(SL0(nsteps:-1:1))]';
    ymin=min(y(:,2));            % Minimum for normalisation of log-polar
plot
    y(:,2)=y(:,2)-ymin;
figure;
    polar(y(:,1),y(:,2)),
    title(sprintf('No-Peak Scattering Diagram: m=%g+%gi, x=%g, min(dB)=
%g',m1,m2,x,ymin)),
    xlabel('Scattering Angle (deg)');
figure;
subplot(2,1,1);
    semilogy(tetad,Ss,'k-'),
    title(sprintf('Mie Angular Scattering: m=%g+%gi, x=%g',m1,m2,x)),
    xlabel('Scattering Angle'),
    ylabel('S');
subplot(2,1,2);
    plot(tetad,dSs,'k-'),
    xlabel('Scattering Angle'),
    ylabel('Polarisation Degree ');
figure;
    semilogy(tetad(nstart:nsteps),Ss(nstart:nsteps),'r:',tetad,S0s,'k-'),
    title(sprintf('No-Peak Angular Scattering: m=%g+%gi, x=%g',m1,m2,x)),
    xlabel('Scattering Angle'),
    ylabel('S0');
figure;
    xmin=min(tetad/180);
    semilogx(tetad/180,z,'r-',tetad/180,z0,'k--',tetad/180,z-z0,'b:'),
    xlabel('Maximum Scattering Angle/180•'),
    axis([xmin, 1, 0, 1.1]);
end;
result.s=[tetad',SR',SL',SR0',SL0',SD',dS',z',z0'];
result.Q=[Qext,Qsca,Qabs,Qb,Qd,asy];
result.gi=gi;
result.g0i=g0i;
```

The MATLAB Function *mie_teta*

```
function result = mie_teta(m, x, tetadlim)

% Computation of Mie Efficienicies and gi coefficients of Legendre
% Polynomial decomposition for complex refractive-index ratio m=m'+im",
% size parameters x=k0*a, scattered intensity with and without
% diffraction peak.
% tetadlim (deg): Optional value of integration limit for
% for beam and diffraction efficiencies (default 180°)
% Output.etab: etab(180°), etab0(180°), etab(tetadlim)
% Output.Q: Qext, Qsca, Qabs, Qb, Qd, Qdlim, asy
% Output.gi and Output.g0i Legendre Coefficients
% C. Mätzler, April 2004.

nsteps=round(23*x);
if nargin==2,
    tetadlim=180;
end;
nx=(1:nsteps); dteta=pi/nsteps;
Q=mie(m,x);  Qext=Q(1); Qsca=Q(2); Qabs=Q(3); Qb=Q(4); asy=Q(5);
nmax=round(2+x+4*x^(1/3));
ab=mie_ab(m,x); an=ab(1,:); bn=ab(2,:);
teta=(nx-0.5).*dteta; tetad=teta*180/pi;
u=cos(teta); s=sin(teta);
px=pi*x^2;
st=pi*s*dteta/Qsca;      % Constant factor of angular integrands
for j = 1:nsteps,
    pt=mie_pt(u(j),nmax);
    pin =pt(1,:);
    tin =pt(2,:);
    n=(1:nmax);
    n2=(2*n+1)./(n.*(n+1));
    pin=n2.*pin; tin=n2.*tin;
    S1=(an*pin'+bn*tin');
    S2=(an*tin'+bn*pin');
    xs=x.*s(j);
    if abs(xs)<0.00002   % Diffraction pattern according to BH, p. 110
        S3=x.*x*0.25.*(1+u(j));    % avoiding division by zero
    else
        S3=x.*x*0.5.*(1+u(j)).*besselj(1,xs)./xs;
    end;
    S4=S1-S3;
    S5=S2-S3;
    SR(j)= real(S1'*S1)/px;
    SL(j)= real(S2'*S2)/px;
    SR0(j)=real(S4'*S4)/px;
    SL0(j)=real(S5'*S5)/px;
end;
z=st.*(SL+SR);       % Integrand
z0=st.*(SL0+SR0);    % Integrand
etabdlim=cumsum(z);  % Beam Efficiency with limited angle
nj=11;
for jj=1:nj,         % Phase fct. decomposition in Legendre Polynomials
    xa=legendre(jj-1,u);  % Legendre Function
    x0=xa(1,:);      % Legendre Polynomial
    gi(jj)=x0*z';    % Beam Eff., asymmetry factor and higher gi's
    g0i(jj)=x0*z0';  % same, but diffraction signal removed
end;
etab=gi(1);     gi=gi/etab;     gi=gi(2:nj);
etab0=g0i(1);   g0i=g0i/etab0;  g0i=g0i(2:nj);
Qd=Qsca*(etab-etab0);      % Diffraction efficiency
n=max(find(tetad<tetadlim));
Qdlim=Qsca*etabdlim(n);    % Limited diffraction efficiency

result.etab=[etab, etab0, etabdlim(n)];
result.Q=[Qext, Qsca, Qabs, Qb, Qd, Qdlim, asy];
result.gi=gi;
result.g0i=g0i;
```

The MATLAB Function *mie_ phasefunction*

```
function result = mie_phasefunction(m, x, u, peak)

% Computation of Mie Phase Function p=p1+p2 (unpolarised)
% with normalisation to 'one' when integrated
% over all directions/(4*pi), see Eq. (28) of Chandrasekhar
% 1960, with complex refractive index m=m'+im",
% size parameter x=k0*a, and u=cos(scattering angle),
% where k0=vacuum wave number, a=sphere radius;
% peak=0 if diffraction signal is to be subtracted
% s. p. 111-114 of Bohren and Huffman (1983) BEWI:TDD122
% C. Mätzler, July 2003, revised April 2004.

nmax=round(2+x+4*x^(1/3));
ab=mie_ab(m,x);
an=ab(1,:);
bn=ab(2,:);

pt=mie_pt(u,nmax);
pin =pt(1,:);
tin =pt(2,:);

n=(1:nmax);
n2=(2*n+1)./(n.*(n+1));
pin=n2.*pin;
tin=n2.*tin;
S1=(an*pin'+bn*tin');
S2=(an*tin'+bn*pin');
if peak==0,
% Computation of diffraction pattern S according to BH, p. 110
    xs=x.*sqrt(1-u.*u);
    if abs(xs)<0.0001
        S=x.*x*0.25.*(1+u);        % avoiding division by zero
    else
        S=x.*x*0.5.*(1+u).*besselj(1,xs)./xs;
    end;
    S1=S1-S;
    S2=S2-S;
end;
Q=mie(m,x);
Qext=Q(1); Qsca=Q(2); asy=Q(5); w0=Qsca/Qext;
p=2*(S1'*S1+S2'*S2)/(Qsca*x^2);
% Qsca to be exchanged by Qext above if normalisation to
% single-scattering albedo, w, is required
result=[p,w0,asy];
```